



Aalborg Universitet

AALBORG UNIVERSITY  
DENMARK

## Machine learning based downscaling of GRACE-estimated groundwater in Central Valley, California

Agarwal, Vibhor ; Akyilmaz, Orhan ; Shum, CK; Feng, Wei; Yang, Ting-Yi ; Forootan, Ehsan; Syed, Tajdarul Hassan ; Haritashya, Umesh K. ; Uz, Metehan

*Published in:*  
Science of the Total Environment

*DOI (link to publication from Publisher):*  
[10.1016/j.scitotenv.2022.161138](https://doi.org/10.1016/j.scitotenv.2022.161138)

*Creative Commons License*  
CC BY-NC-ND 4.0

*Publication date:*  
2023

*Document Version*  
Accepted author manuscript, peer reviewed version

[Link to publication from Aalborg University](#)

*Citation for published version (APA):*  
Agarwal, V., Akyilmaz, O., Shum, CK., Feng, W., Yang, T.-Y., Forootan, E., Syed, T. H., Haritashya, U. K., & Uz, M. (2023). Machine learning based downscaling of GRACE-estimated groundwater in Central Valley, California. *Science of the Total Environment*, 865, Article 161138. <https://doi.org/10.1016/j.scitotenv.2022.161138>

### General rights

Copyright and moral rights for the publications made accessible in the public portal are retained by the authors and/or other copyright owners and it is a condition of accessing publications that users recognise and abide by the legal requirements associated with these rights.

- Users may download and print one copy of any publication from the public portal for the purpose of private study or research.
- You may not further distribute the material or use it for any profit-making activity or commercial gain
- You may freely distribute the URL identifying the publication in the public portal -

### Take down policy

If you believe that this document breaches copyright please contact us at [vbn@aub.aau.dk](mailto:vbn@aub.aau.dk) providing details, and we will remove access to the work immediately and investigate your claim.



# **Machine learning based downscaling of GRACE-estimated groundwater in Central Valley, California.**

Vibhor Agarwal<sup>1,2,3</sup>, Orhan Akyilmaz<sup>4</sup>, C.K. Shum<sup>3,5</sup>, Wei Feng<sup>5,6</sup>, Ting-Yi Yang<sup>7</sup>, Ehsan Forootan<sup>8</sup>, Tajdarul Hassan Syed<sup>9</sup>, Umesh K. Haritashya<sup>2</sup>, Metehan Uz<sup>3</sup>

<sup>1</sup> Department of Earth Sciences, College of Wooster, USA

<sup>2</sup> Department of Geology and Environmental Geosciences, University of Dayton, USA

<sup>3</sup> Division of Geodetic Science, School of Earth Sciences, The Ohio State University, USA

<sup>4</sup> Department of Geomatic Engineering, Istanbul Technical University, Turkey

<sup>5</sup> Innovation Academy for Precision Measurement Science and Technology, Chinese Academy of Sciences, China

<sup>6</sup> School of Geospatial Engineering and Science, Sun Yat-sen University, China;

<sup>7</sup> Polaris Geospatial Services, Columbus, Ohio, USA;

<sup>8</sup> Department of Planning, Aalborg University, Denmark;

<sup>9</sup> Department of Earth Sciences, Indian Institute of Technology Kanpur, India

Corresponding Author: Vibhor Agarwal, [agarwal.282@osu.edu](mailto:agarwal.282@osu.edu) [agarwal.vibhor.phd@gmail.com](mailto:agarwal.vibhor.phd@gmail.com)

1  
2  
3  
4  
5  
6  
7  
8  
9  
10  
11  
12  
13  
14  
15  
16  
17  
18  
19  
20

**Machine learning based downscaling of GRACE-estimated groundwater in  
Central Valley, California.**

Vibhor Agarwal<sup>1,2,3</sup>, Orhan Akyilmaz<sup>4</sup>, C.K. Shum<sup>3,5</sup>, Wei Feng<sup>5,6</sup>, Ting-Yi Yang<sup>7</sup>, Ehsan  
Forootan<sup>8</sup>, Tajdarul Hassan Syed<sup>9</sup>, Umesh K. Haritashya<sup>2</sup>, Metehan Uz<sup>3</sup>

- <sup>1</sup> Department of Earth Sciences, College of Wooster, USA
- <sup>2</sup> Department of Geology and Environmental Geosciences, University of Dayton, USA
- <sup>3</sup> Division of Geodetic Science, School of Earth Sciences, The Ohio State University, USA
- <sup>4</sup> Department of Geomatic Engineering, Istanbul Technical University, Turkey
- <sup>5</sup> Innovation Academy for Precision Measurement Science and Technology, Chinese Academy  
of Sciences, China
- <sup>6</sup> School of Geospatial Engineering and Science, Sun Yat-sen University, China;
- <sup>7</sup> Polaris Geospatial Services, Columbus, Ohio, USA;
- <sup>8</sup> Department of Planning, Aalborg University, Denmark;
- <sup>9</sup> Department of Earth Sciences, Indian Institute of Technology Kanpur, India

Corresponding Author: Vibhor Agarwal, [agarwal.282@osu.edu](mailto:agarwal.282@osu.edu) [agarwal.vibhor.phd@gmail.com](mailto:agarwal.vibhor.phd@gmail.com)

21 **Abstract**

22 California's Central Valley, one of the most agriculturally productive regions, is also one of the  
23 most stressed aquifers in the world due to anthropogenic groundwater over-extraction primarily  
24 for irrigation. The groundwater depletion is further exacerbated by climate-stressed droughts.  
25 Gravity Recovery and Climate Experiment (GRACE) satellite gravimetry has demonstrated the  
26 feasibility of quantifying global groundwater storage changes at uniform monthly sampling,  
27 though at a coarse resolution and is thus impractical for effective water resources  
28 management). Here, we employ the Random Forest machine learning algorithm to establish  
29 empirical relationships between GRACE-derived groundwater storage and in-situ groundwater  
30 level variations over the Central Valley during 2002–2016 and achieved downscaling of  
31 GRACE-observed groundwater storage changes from 666 km to 5 km. Validations of our  
32 modeled groundwater level with *in situ* groundwater level indicate excellent Nash-Sutcliffe  
33 Efficiency coefficients ranging from 0.94–0.97. In addition, the modeled groundwater trends  
34 have good agreements with two independent measurements of vertical land subsidence  
35 measured rates using GPS, and CryoSat-2 radar altimetry. Our estimated groundwater loss is  
36 about 30 km<sup>3</sup> during 2002–2016, which agrees well with previous studies. We find the maximum  
37 groundwater storage losses of  $-5.7 \pm 1.2 \text{ km}^3 \text{ yr}^{-1}$  and  $-9.8 \pm 1.7 \text{ km}^3 \text{ yr}^{-1}$  occurred during the  
38 extended drought periods of January 2007-December 2009, and October 2011-September  
39 2015, respectively. We observed that Central Valley experienced groundwater recharges during  
40 abrupt winter flood episodes. The 5-km resolution Central Valley-wide groundwater storage  
41 trends reveal that groundwater depletion occurs mostly in southern San Joaquin Valley and is  
42 collocated with sites showing severe land subsidence due to aquifer compaction from  
43 groundwater over withdrawal.

44 **Keywords:** Machine Learning, Groundwater, GRACE, Remote Sensing

45 **1. Introduction**

46 Groundwater is an important freshwater resource that meets agricultural, industrial, and  
47 domestic needs (Siebert et al., 2010; Wada et al., 2014; Zekster and Everett, 2004). Over the  
48 past few decades, several aquifers worldwide such as Central Valley, High Plains, Indus Plain,  
49 middle East, and others, have faced unprecedented human-induced stress due to the  
50 population growth, expansion of the irrigated areas, and other economic activities causing a  
51 drastic increase in groundwater usage (Bierkens and Wada, 2019; Famiglietti, 2014).  
52 Groundwater abstraction and outflow exceeding groundwater recharge over a long period of  
53 time and in large areas has been reported as the main cause of groundwater depletion  
54 (Konikow and Kendy, 2005; Wada et al., 2010). Groundwater depletion can lead to global water  
55 security and environmental issues (Famiglietti, 2014; Wada et al., 2010). There is an urgent  
56 need for quantifying long-term groundwater storage variations (GWS) at frequent temporal  
57 samplings that can help characterize the groundwater depletion in these stressed regions.

58 Several approaches for quantifying GWS variations have been applied (e.g., Bierkens and  
59 Wada, 2019). Groundwater levels from *in-situ* ground wells provide essential information about  
60 stresses acting on the aquifers and play a key role in developing groundwater models (Taylor  
61 and Alley, 2001). Continuous groundwater level observations may further help quantify GWS  
62 and predict future trends in storage (Butler et al., 2013; Sun et al., 2013). However, it is  
63 infeasible to use only these data for quantifying regional GWS for several reasons. Firstly,  
64 monitoring wells required to accurately estimate groundwater levels are expensive to install and  
65 maintain. Therefore, several aquifers have poor coverage of such wells. Secondly, spatio-  
66 temporal gaps in the coverage of ground wells might necessitate the interpolation of  
67 groundwater level data, leading to interpolation errors (Ahamed et al., 2022; Thomas et al.,  
68 2017). Thirdly, uncertainties in the value of storage coefficient at well sites might translate into  
69 errors in GWS (Scanlon et al., 2012; Alam et al., 2021). Since 2002, the Gravity Recovery and  
70 Climate Experiment (GRACE) twin-satellite mission gravimetry data have enabled a continuous

71 global Terrestrial Water Storage (TWS) record for over a decade and a half, at a spatial  
72 resolution larger than 333 km (half-wavelength) and monthly sampling, e.g., Frappart et al.,  
73 (2018). Innovative processing of GRACE data has enabled the uniform global quantification of  
74 GWS change for the first time by removing surface water storage changes using hydrologic data  
75 and model outputs (Famiglietti et al., 2011; Rodell et al., 2009), as well as data assimilation (50  
76 km resolution in Mehrnegar et al., (2021); 12.5 km resolution in Schumacher et al., (2018)).  
77 However, due to the limited spatial resolution and the associated errors in disaggregating  
78 GRACE-derived TWS (Scanlon et al., 2012), the application of GRACE data directly for  
79 groundwater assessment is not feasible at the local scale (Alley and Konikow, 2015), including  
80 in Central Valley in California which is the subject of the present study. Moreover, most GRACE-  
81 based groundwater studies estimate GWS variations by removing soil moisture estimates  
82 simulated by Land Surface Models (LSMs) from GRACE observations of terrestrial water  
83 storage (Scanlon et al., 2012). However, LSMs do not simulate irrigation water use; hence soil  
84 moisture values will be particularly erroneous in the Central Valley, where groundwater irrigation  
85 is predominant (Famiglietti et al., 2011).

86 Other methods of GWS computation include the water balance method, where several hydro-  
87 meteorologic quantities, such as the difference between stream inflow and outflow, precipitation,  
88 and evapotranspiration, along with several of the storage changes (soil moisture, snow water  
89 equivalent, reservoir storage) are computed for a given aquifer (Ahamed et al., 2022; Xiao et al.,  
90 2017). Several remote sensing, in-situ, and modeled datasets can be used to estimate the  
91 above quantities. However, these quantities might be subject to sources of uncertainties that  
92 creep into the water balance equation (Ahamed et al., 2022; Bierkens and Wada, 2019).  
93 Further, vertical deformation from GPS and Interferometric Synthetic Aperture Radar (InSAR)  
94 can provide regional estimates of groundwater storage changes (Ojha et al., 2018) or trends in  
95 the case of InSAR. With the availability of Sentinel-1 data since 2014, this method holds

96 promise for revealing aquifer dynamics and storage variations at high spatial resolutions  
97 (Castellazzi et al., 2016; Vasco et al., 2021). However, often in lieu of missing a continuous and  
98 uniform time series, InSAR land velocity or trend/subsidence estimates could potentially be  
99 biased due primarily to interannual or longer signals in the land deformation data.

100 Machine Learning (ML) has been used for solving several non-linear complex problems in  
101 geoscience, e.g., Dramsch et al. (2020) and Sun and Scanlon (2019), as it does not require the  
102 knowledge of exact physical relationships between input and target variables. Machine Learning  
103 can also be used to estimate GWS variations at a higher resolution if GRACE-derived TWS  
104 variations can be downscaled to model in-situ groundwater level variations. A suitable  
105 combination of hydro-meteorological variables should be identified as input variables to build a  
106 robust machine-learning algorithm to model groundwater variations (Adamowski and Chan,  
107 2011). Several studies in the past have incorporated machine learning models like Artificial  
108 Neural Network (ANN) model, Random Forest, Boosted Regression Tree, and Deep Learning to  
109 downscale GRACE satellite data to produce GWS variations at high resolution (Chen et al.,  
110 2019; Chen et al., 2020; Miro and Famiglietti, 2018; Rahaman et al., 2020).

111 Quantifying GWS variations is especially important for Central Valley. Here, ever-increasing  
112 irrigation demands, limited availability of surface water, and climate extremes such as prolonged  
113 and intensified droughts resulting from climate change have forced farmers to depend more on  
114 groundwater. As a result of the continuing groundwater depletion, several adverse impacts such  
115 as falling groundwater levels, decreasing groundwater yields, increase in pumping costs,  
116 degrading water quality, and damage to the aquatic ecosystems and wetlands have been  
117 observed (Faunt, 2009; Faunt and Sneed, 2015; Konikow, 2015). San Joaquin Valley, a major  
118 agricultural region in Central Valley, has witnessed the largest share of such adverse impacts,  
119 which have become more severe during prolonged and recurrent droughts in California.



120 Several of the methods mentioned above have been applied to quantify the GWS in Central  
121 Valley. Famiglietti et al., (2011) used GRACE-derived TWS variations and other hydrological  
122 variables to quantify GWS variations during 2002-2011. Scanlon et al., (2012) used updated  
123 GRACE processing and in-situ groundwater level variations to compute groundwater depletion  
124 from 2002-2011. Ojha et al., (2018) used vertical deformation derived from InSAR to derive the  
125 storage changes. Alam et al., (2021) used a combination of GRACE, wells, water balance, and  
126 hydrological modeling to quantify GWS variations from 2003-2019. Ahamed et al., (2022) used  
127 remote sensing data and an ensemble of water balance methods to quantify groundwater  
128 storage variations in Central Valley during 2002-2020. Miro and Famiglietti, (2018) implemented  
129 ANN using GRACE-derived TWS variations along with hydro-meteorologic variables to model  
130 annual amplitudes of GWS variations at 4 km spatial resolution over a small portion of the San  
131 Joaquin Valley in Central Valley during 2002-2010. All the above studies have confirmed the  
132 continued loss of groundwater losses along with dramatic rates of subsidence due to  
133 groundwater overdrafts during the last two decades.

134 All the above methods, except those utilizing in-situ wells and machine learning techniques,  
135 have limited capability to model GWS variations at high spatial resolutions at frequent temporal  
136 intervals. Groundwater levels in Central Valley can reflect complex variations due to withdrawal  
137 for irrigation, recharge due to partial infiltration of irrigation water, surface water impoundment,  
138 or precipitation. Further, climate extremes such as drought have put unprecedented stress on  
139 groundwater reserves which might be reflected in the groundwater fluctuations (Faunt, 2009).  
140 Compared to interpolation and kriging, more robust approaches are needed to fill the spatio-  
141 temporal gaps in in-situ groundwater levels and possibly obtain regional storage variations  
142 (Alam et al., 2021; Thomas et al., 2017). Previous machine learning-based approaches (Miro  
143 and Famiglietti, 2018) can be further expanded to the whole of Central Valley to cover broader

144 spatio-temporal scales and improve the accuracy of modeled results using a suitable choice of  
145 input variables, models and better approaches for training the machine learning model.

146 The primary objective of this study is to downscale GRACE-derived GWS variations in  
147 Central Valley, California, using the Random Forest machine learning algorithm. We chose the  
148 period from October 2002-September 2016, which covers most of the operational phase of  
149 GRACE satellite data. We use GRACE along with hydro-meteorologic/geologic data as input  
150 and in-situ groundwater level data as the target data for the model. Further, the Central Valley  
151 has a record of geodetic measurements from GPS, extensometers, and remote sensing  
152 observations, which have been used to quantify the subsidence due to groundwater overdraft  
153 (Ojha et al., 2018; Sneed and Brandt, 2015). These data can provide us with ancillary  
154 information against which we can further validate our modeled results as a part of our second  
155 objective. Primarily, we compared the modeled groundwater level with the vertical deformation  
156 obtained from GPS and altimeter and obtained an inelastic storage coefficient for a portion of  
157 Central Valley. This approach of combining multiple hydrological and geodetic data can further  
158 enhance our understanding of aquifer dynamics, which is important for regional studies such as  
159 the one presented here. A machine learning approach might help provide relevant local-scale  
160 data on groundwater depletion to Groundwater Sustainability Agencies (GSAs) to make  
161 informed management decisions required to support the goals of the Sustainable Groundwater  
162 Management Act.

163

## 164 **2. Study area**

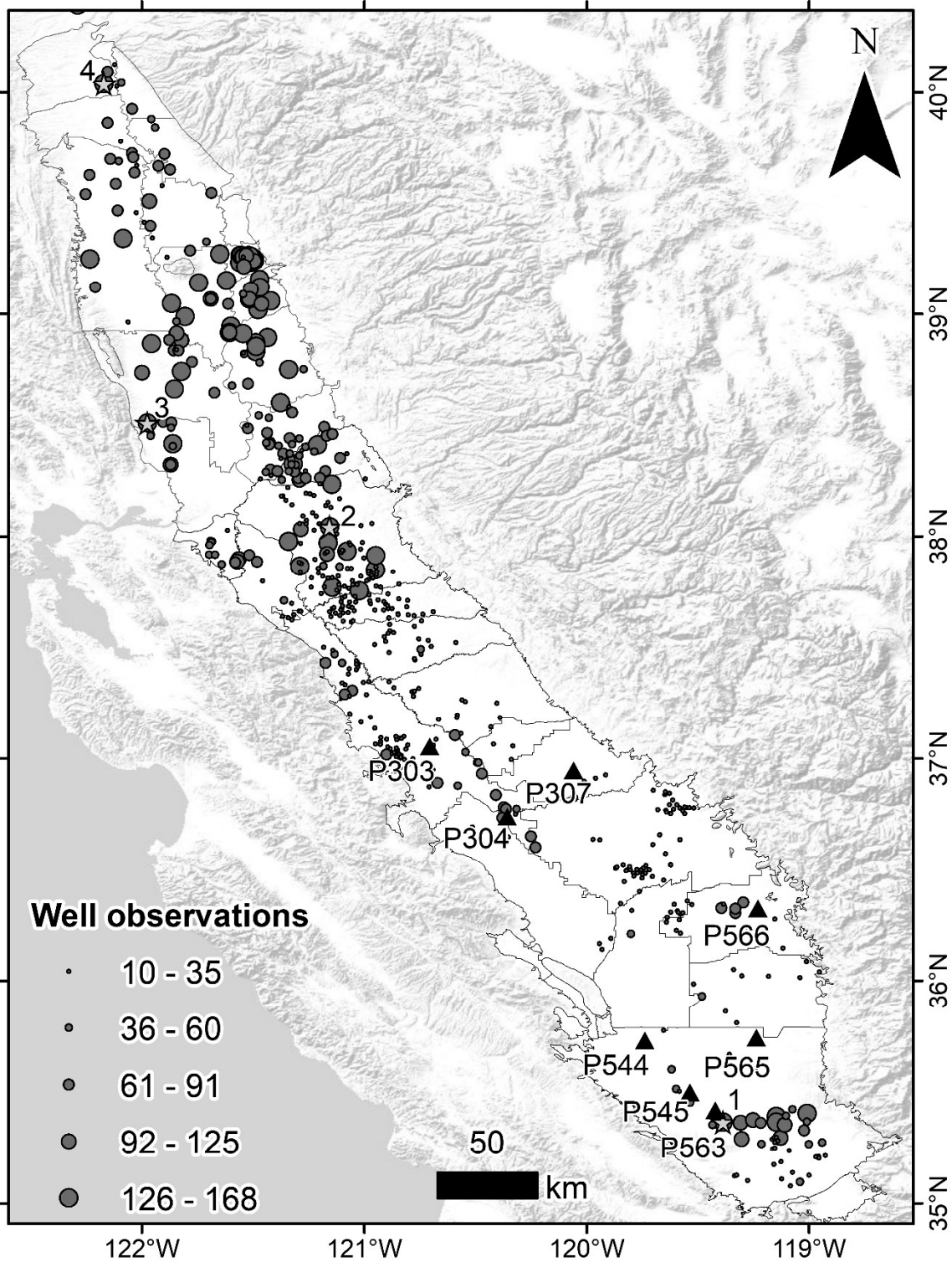
165 The Central Valley aquifer system in California covers an area of 52,000 km<sup>2</sup> (Figure 1) and  
166 produces one-fourth of the food in the US (Faunt, 2009). Central Valley is primarily semi-arid  
167 and most precipitation occurs during the winter and early spring months and not in summer

168 when it is needed for irrigation and drinking (Jasechko et al., 2020). San Joaquin Valley is the  
169 major agricultural region and surface water quantity here depends on seasonal snowmelt from  
170 the Sierra Nevada in the East and Sacramento Valley in the North, which varies from year to  
171 year. Consequently, supplies for irrigation must be met through diverted surface water sources,  
172 and through groundwater from confined and unconfined aquifers. Groundwater is, therefore, an  
173 essential/persistent freshwater source accounting for up to 40% or more of the required water  
174 supply in Central Valley.

175 Central Valley lost approximately 113 km<sup>3</sup> of groundwater in the 20<sup>th</sup> century and 20 percent  
176 of this depletion is estimated to be contributing to land subsidence (Faunt, 2009). Consequently,  
177 groundwater levels have been declining since the 1930s when the first in-situ measurement was  
178 made (Bertoldi, 1989; Williamson et al., 1989). Groundwater storage losses from GRACE  
179 satellite observations and Central Valley Hydrological Model for the first decade of the 21<sup>st</sup>  
180 century is 25-30 km<sup>3</sup> (Konikow, 2013).

181 As groundwater depletion continues in Central Valley and other nearby regions, Sustainable  
182 Groundwater Management Act was passed in 2014 in California to promote better groundwater  
183 management and governance. Through this act, more emphasis is laid on the sustenance of  
184 groundwater resources for all regions by optimizing the water consumption by agricultural and  
185 other sectors. This issue is extremely critical for Central Valley as impacts of depletion here are  
186 visible from the 1920s on the local scale.

187



188

189

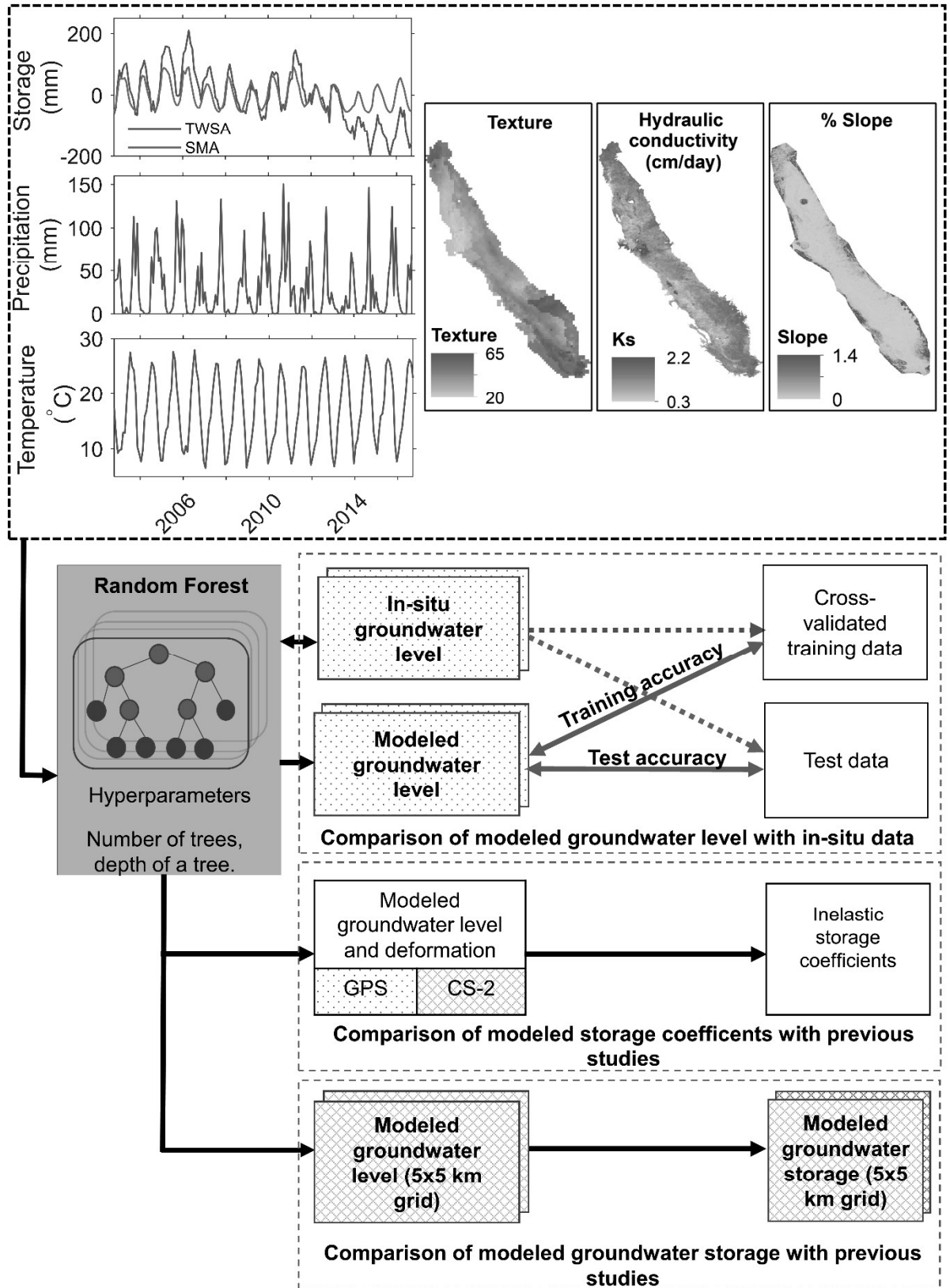
190

**Figure 1.** Location of Central Valley and two major basins, Sacramento (black) and San Joaquin (blue) Valley in north and south, respectively. The location of wells used in this study

191 and the number of measurements over the study period is also shown with filled red circles. 7  
192 GPS sites used in this study are shown by black triangles. The green stars represent the wells  
193 used for plotting in Figure

### 194 **3. Data and Methods**

195 We implemented the Random Forest (RF) machine learning (ML) model and followed the data  
196 processing workflow as in Figure 2.



198 **Figure 2.** The workflow used for modeling groundwater level

199 **3.1. Input and target data**

200

201 **3.1.1. Precipitation and temperature**

202 Here monthly precipitation and temperature data is obtained from Parameter-Elevation  
203 Regression on Independent Slopes Model (PRISM) dataset at 4 km spatial resolution (Daly et  
204 al., 2008). PRISM simulates the spatial variations of the weather and climate using in-situ data.  
205 It uses a “weighted regression scheme” to account for different physiographic features and  
206 climate regimes when providing final estimates of precipitation and temperature.

207 Since precipitation can take a few months to recharge groundwater, we use 0, 1, 2, 3, and 4-  
208 month lags for precipitation labeled as PPT0, PPT1, PPT2, PPT3, and PPT4, respectively, in  
209 this study.

210

211 **3.1.2. Terrestrial Water Storage and Soil Moisture Variations**

212 For the computation of TWS, we used the latest GRACE data product, the Release (RL) 06  
213 Level 2 (L2) monthly gravity field solutions provided by the University of Texas at Austin Center  
214 for Space Research (CSR). This solution consists of monthly spherical harmonic coefficients  
215 (SHC) complete to degree and order 60. This truncation represents low pass filtering in the  
216 spatial domain, causing a limited spatial resolution of GRACE data due to signal dampening.  
217 Consequently, the above processing step causes GRACE signal to represent 666 km (half-  
218 wavelength) resolution on the ground. The post-processing involves standard steps such as  
219 replacing the degree d the zonal degree 2 coefficients from satellite laser ranging solutions,  
220 correcting for Glacial Isostatic Adjustment (GIA) process using a forward model, destriping using  
221 the Swenson method (Swenson and Wahr, 2006), and smoothing using a Gaussian filter of 300

222 km half-radius. Further signal leakage correction is performed by the iterative forward modeling  
223 approach (Chen et al., 2014). More detailed descriptions for GRACE post-processing are  
224 available in supplementary section 1. We finally obtained monthly TWS anomaly grids  
225 oversampled at 0.25° resolution.

226 We obtained the monthly soil moisture from the GLDAS Noah Land Surface Model L4 monthly  
227 0.25° x 0.25° V2.1 (GLDAS\_NOAH025\_M) [accessed October 2020]. We compute soil moisture  
228 anomaly (SMA) by removing the mean soil moisture over the study period. We further computed  
229 TWSA-SMA, which provides useful information on spatio-temporal groundwater storage  
230 variations continuously over the study period covering the whole Central Valley. However, it is  
231 with the coarsest resolution of 0.25° amongst the predictor variables.

232

### 233 **3.1.3. Saturated hydraulic conductivity (K)**

234 Saturated hydraulic conductivity data is available at 1 km spatial resolution (Zhang et al., 2019).  
235 To our knowledge, this is the only publicly available global dataset at such fine resolution.

236

### 237 **3.1.4. Texture**

238 Faunt et al., (2009) compiled texture data from the lithological drill holes, which range in depth  
239 from 12 to 1200 feet below the ground level. Faunt et al., (2009) used this textural data to  
240 simulate the geological model for Central Valley Hydrologic Model.

241

### 242 **3.1.5. Percent Slope**



243 Percent slope is derived from the National Elevation Dataset (NED) at 1/3 arc second (~10 m)  
244 resolution.

245

### 246 **3.1.6. Groundwater level**

247 The target variable against which we train for our machine learning model is the in-situ  
248 groundwater level obtained from the California Department of Water Resources (DWR)  
249 California Statewide Groundwater Elevation Monitoring (CASGEM) database (DWR CASGEM,  
250 2021 a, b) and the United States Geological Survey (<http://water.usgs.gov/ogw/data.html>).  
251 Though Central Valley consists of ~10,000 wells, we chose 586 wells for the entire Central  
252 Valley with good spatio-temporal coverage over our study period. We only chose a well if it has  
253 at least biannual measurement or continuous measurement over a shorter time scale within our  
254 study period (Figure 1).

255

### 256 **3.1.7. Deformation data**

257 The vertical deformation data from GPS and CryoSat-2 (CS2) radar altimeter was not used for  
258 ML model development but rather as independent data to validate our modeled groundwater  
259 level results. GPS data is available from  
260 [https://sideshow.jpl.nasa.gov/pub/JPL\\_GPS\\_Timeseries/repro2018a/post/point/](https://sideshow.jpl.nasa.gov/pub/JPL_GPS_Timeseries/repro2018a/post/point/), NASA Jet  
261 Propulsion Laboratory (JPL), California Institute of Technology. We also use the CS2 low-  
262 resolution mode (LRM) radar altimetry data sensing solid Earth deformation time series in an  
263 innovative method applied to Central Valley (Yang, 2020). CS2 data was waveform retracked  
264 and spatially interpolated to obtain the 2-D vertical deformation maps for the southern San  
265 Joaquin Valley (Figure S1).

266 Finally, to overcome the problem of mismatch in the spatial resolution of various input and target  
267 variables, all the inputs except the TWSA-SMA are interpolated at the ground well locations  
268 using the 'scatteredInterpolant' function in MATLAB and all input variables were aggregated to  
269 monthly sampling. The variable TWSA-SMA is used without further interpolations or resampling  
270 at the 0.25° spacing interval.

271

## 272 **3.2. Machine Learning Modeling**

273

### 274 **3.2.1. Random Forest**

275 Random Forest is a robust model which has shown the capability to produce highly accurate  
276 results for several geological applications, e.g., Hengl et al., (2018) and Tyrallis et al., (2019).

277 Random Forest is an ensemble of decision trees (DTs) consisting of decision-making units  
278 known as nodes arranged in the form of a tree. Each DT is trained by passing data down from  
279 the node at the top (root node) to the leaf node (the node at which splitting stops), each splitting  
280 of a node result in two child nodes. Out of all the input variables at a node, the one chosen for  
281 splitting should be such that the child nodes are "purer", i.e., homogeneous in terms of the  
282 target variable than the parents. The metric that is commonly used in regression problems is the  
283 sum of squared error (SSE) between all the observations at a particular node, and the mean of  
284 all the observations. Thus, SSE should be lower for the child nodes compared to the parent  
285 nodes for a valid split.

286 In the algorithm described in Breiman, (2001), the observations are randomly sampled with  
287 replacement at each DT, a process known as bagging. Approximately two-thirds of observations  
288 are used for model building in each DT and are known as "in-bag" samples. The remaining one-  
289 third of the samples are called "out of bag" (OOB) samples used for internal validation by the RF

290 model. Each DT has a different combination of in-bag and OOB data, and by combining  
291 predictions on OOB data from each DT, we can get a secondary validation of whether our RF  
292 model is over-fitted. Randomness in an RF is further increased by only selecting a few input  
293 variables for each DT, reducing the correlation between individual DTs and preventing  
294 overfitting.

295

### 296 **3.2.2. Development of model**

297 During the development of any machine learning model, a small portion of the dataset is  
298 isolated, known as the test dataset. The remaining dataset is then split into a training dataset,  
299 using which a model is built, and a validation dataset, against which the accuracy of the model  
300 is evaluated. This process of developing and fine-tuning the model on the training and validation  
301 dataset is iterative and repeated until the desired number of steps or accuracy is achieved. The  
302 predictive accuracy of the model is evaluated against the independent test dataset. Here we  
303 randomly select a test dataset spread throughout the study period and it constitutes 20% of the  
304 overall dataset. Previous studies have used 10-44% of the overall dataset as test data (Rajae  
305 et al., 2019).

306

### 307 **3.2.3. Cross-validation of model**

308 Several studies (Hawkins et al., 2003; Molinaro et al., 2005) have pointed out that for smaller  
309 sample sizes, a single validation dataset does not provide an unbiased estimate of model  
310 performance. We, therefore, use the k-fold cross-validation technique wherein a training dataset  
311 is further split into multiple folds, each containing a unique combination of training and validation  
312 dataset. A separate model is then built and evaluated for each fold of the data. This way, model  
313 parameters are optimized for the entire dataset and overfitting is minimized. Finally, an

314 ensemble of models is formed, and their predictive accuracy is quantified with the test dataset.  
315 Since k-fold cross validation makes machine learning model development slower, we use k=5 or  
316 5-fold for model development.

317

#### 318 **3.2.4. Hyperparameter optimization**

319 Random Forest model has several hyperparameter values which need to be initialized by the  
320 user (Biau and Scornet, 2016; Probst and Boulesteix, 2017). They include the number of  
321 decision trees, the number of samples in the leaf node, and the number of variables to consider  
322 for splitting in each decision tree. While previous studies have attempted to improve machine  
323 learning predictions by increasing the complexity of model architecture (Nourani et al., 2013;  
324 Seyoum et al., 2019; Yin et al., 2022) or by optimizing the number of input variables (Rajaei et  
325 al., 2019; Tyralis and Papacharalampous, 2019), fewer studies have implemented strategies for  
326 optimizing hyperparameters. While random search and grid search algorithms for  
327 hyperparameter optimization are time-consuming and might not lead to the best  
328 hyperparameters (Feurer and Hutter, 2019; Yin et al., 2021), we fine-tune the machine learning  
329 models by implementing a Bayesian Hyperparameter Optimization (Snoek et al., 2012). This  
330 optimization algorithm first builds a probability model of the objective function (such as RMSE)  
331 during model training using different hyperparameters. It then uses the Bayesian distribution to  
332 find the most promising hyperparameter to evaluate the true (actual) objective function.

333

#### 334 **3.2.5. Assessment of model accuracy and feature importance**

335 The modeled results are validated against selected *in situ* groundwater level observations  
336 located in the Central Valley using statistical estimates, correlation coefficient, root mean  
337 squared error (RMSE), Nash-Sutcliffe efficiency (NSE) coefficient, and scaled RMSE ( $R^*$ ).

338 Supplementary section contains detailed information on these quantities. Correlation quantifies  
339 the interdependence between two datasets. It ranges in value from  $-1$  to  $+1$ , which represents a  
340 perfect negative and positive relationship, respectively, while a value of  $0$  represents no  
341 relationship. RMSE quantifies the standard deviation of residuals of the best fit line between  
342 observed and modeled values. NSE has been used to quantify the predictive power of  
343 hydrological models (Nash and Sutcliffe, 1970) and ranges from  $-\infty$  to  $+1$ . Values below  $0$  suggest  
344 unacceptable predictions, while above  $0$  are good predictions, with  $1$  being the perfect  
345 prediction.

346 We also compute the feature importance by permuting out of bag (OOB) observations (Breiman,  
347 2001). The underlying concept of this approach is that permuting the values of the most  
348 influential predictor should lead to the most increase in modeling error.

349 To further understand the dependence of modeling accuracy of the model on the input  
350 variables, we use the drop-column method (Jyolsna et al., 2021; Parr et al., 2020). We consider  
351 the model developed above after Bayesian Hyperparameter Optimization using all the input  
352 variables as the base model. Models are retrained without the dropped input variables and the  
353 increase in RMSE on test data compared to the base model is noted.

354

### 355 **3.3. Computation of inelastic storage coefficient and groundwater storage**

356 We use the modeled monthly groundwater level variations obtained above and the vertical  
357 deformation data from GPS and CS-2 altimeter to obtain the inelastic storage coefficient  $S_{kv}$ .  
358 The formula for computing  $S_{kv}$  is mentioned in Supplementary section 3. Since GPS measures  
359 daily vertical deformation, we averaged them to monthly values when correlating them with  
360 monthly groundwater level.

361 For unconfined aquifers, the storage coefficient is the specific yield ( $S_y$ )—the volume of water  
362 released due to drainage from an unconfined aquifer per unit decline in groundwater level. In  
363 the Central Valley, typical values range from 0.06 to 0.3 (Faunt, 2009). We obtained the  
364 groundwater storage in terms of equivalent water height (EWH) for the whole of Central Valley  
365 by multiplying groundwater level changes with the specific yield of 0.1 for the unconfined wells  
366 (<60 m deep) (Faunt, 2009). The groundwater storage, when multiplied by the area of Central  
367 Valley (~52,000 km<sup>2</sup>), gives the volumetric GWS estimate of Central Valley.

368

## 369 **4. RESULTS**

370

### 371 **4.1 Overall results**

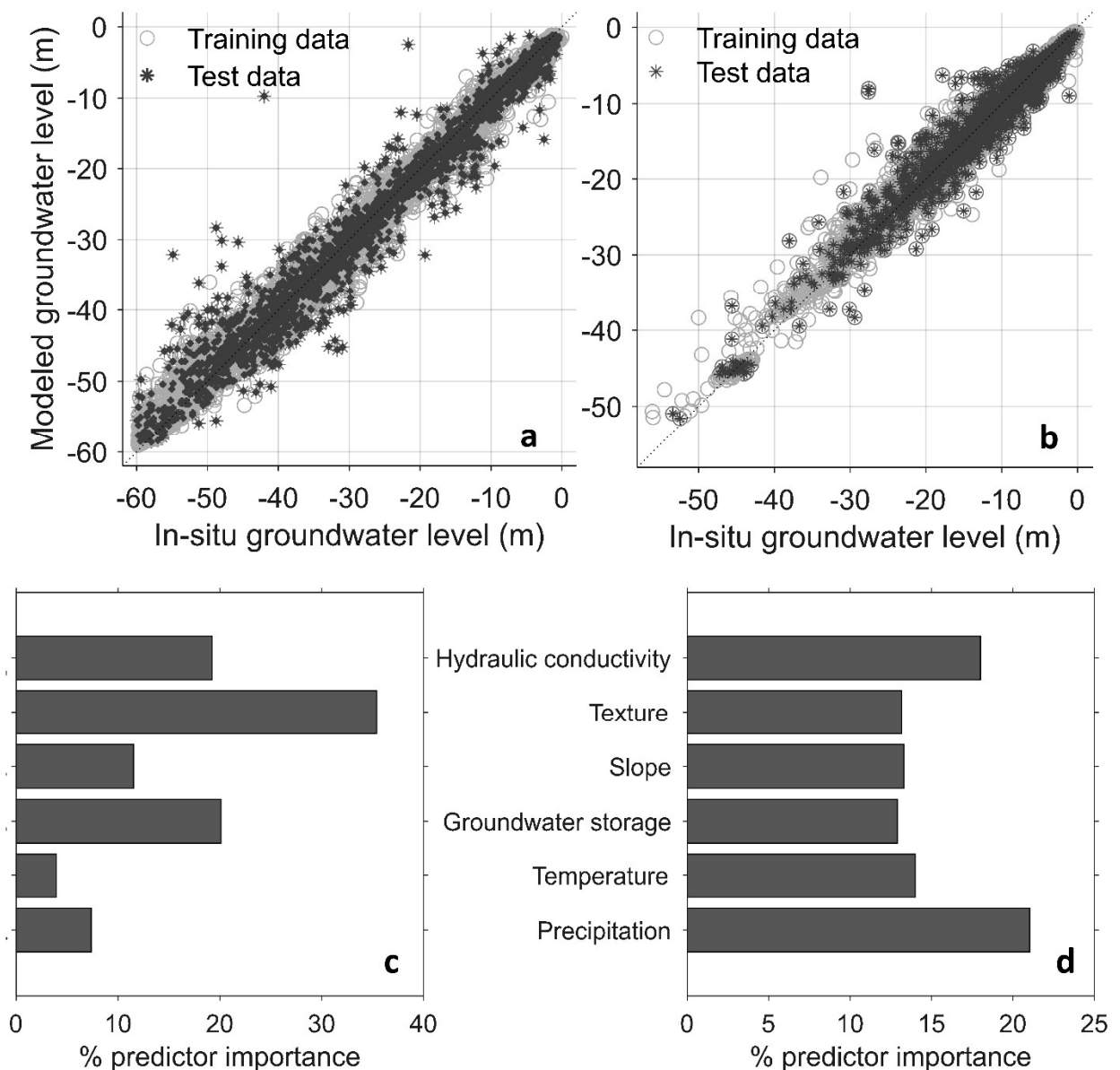
372 Modeled results show a high accuracy for both San Joaquin and the Sacramento Valley (Figure  
373 3a). For San Joaquin Valley, correlation, root mean square error, NSE, and  $R^*$  for training (test)  
374 data are 0.99(0.97), 1.35 (2.72), 0.99 (0.95), and 0.12(0.21), respectively. For Sacramento  
375 valley, correlation, root mean square error, Nash Sutcliffe efficiency, and normalized RMSE for  
376 training (test) data is 0.99(0.95), 1.21(2.12), 0.98(0.94), and 0.14(0.26), respectively. Additional  
377 validations of modeled results with respect to the out-of-bag data are provided in Supplementary  
378 file (Figure S2, Table S1).

379 For the computation of feature importance in Figure 3b, we summed the contributions from  
380 different lags of precipitation, i.e., PPT0, PPT1, PPT2, PPT3 and PPT4, in terms of one  
381 variable, PPT, to make it easier for analysis (Figure S3, we show feature importance  
382 considering all lag components for precipitation). For San Joaquin Valley, texture, hydraulic  
383 conductivity, slope, GWS (TWSA-SMA), temperature and precipitation are the most important  
384 features in decreasing order. For Sacramento Valley, precipitation is the most important,

385 followed by hydraulic conductivity and temperature. Texture, slope and groundwater storage  
386 (TWSA-SMA) show almost similar importance.

387 Using the drop-column method, we find that groundwater storage causes the most increase in  
388 RMSE compared to the base model for both Sacramento and San Joaquin valley (Table S2).

389 Removal of geological factors, texture and hydraulic conductivity, along with topographic slope,  
390 also significantly increases the RMSE of the models.

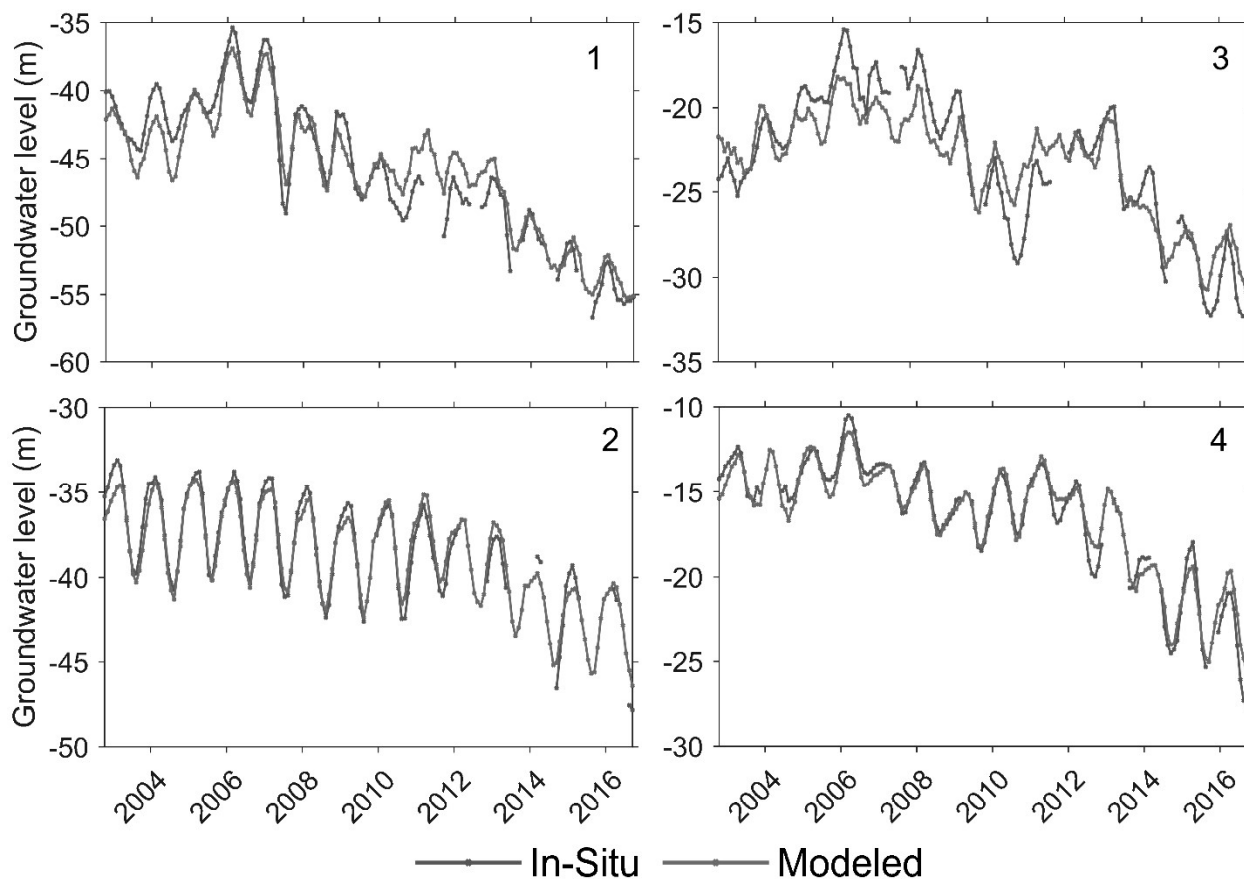


391  
392

**Figure 3.** The accuracy assessment for machine learning modeling. Correlation plots

393 between the modeled results and in-situ groundwater level variations for training and test  
394 data for (a) San Joaquin and (b) Sacramento Valley respectively. Feature importance plots  
395 for (c) San Joaquin and (d) Sacramento Valley.

396  
397 The modeled results also compare well with the *in-situ* groundwater level from several  
398 ground wells (Figure 1, Figure S3) as they show similar seasonality and trends, and the  
399 largest groundwater level declines can be seen during the drought periods (Figure 4, Figure  
400 S4). Some mismatches can be seen, and they indicate that the modeled results are not  
401 perfect. These reflect remaining unmitigated errors or noise in in-situ data which cannot be  
402 modeled. Wells in San Joaquin valley generally show higher declines than those in  
403 Sacramento valley. We can also effectively fill the data gaps in in-situ groundwater levels  
404 through machine learning modeling.



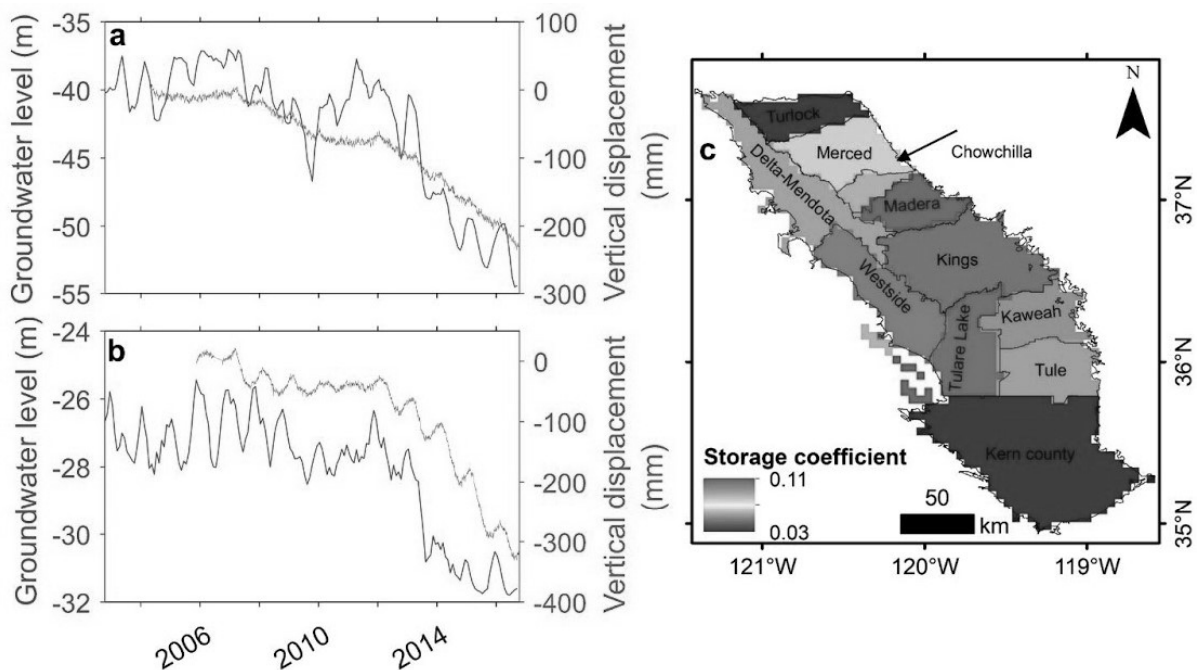


406 **Figure 4.** Modeled and in-situ groundwater level time series for wells in San Joaquin (left)  
407 and Sacramento valley (right). The location of the wells can be seen in Figure 1. Table S3  
408 shows the statistic).

409

#### 410 **4.2 Comparison of modeled results with vertical deformation data**

411 Inelastic storage coefficients from vertical deformation measured at GPS sites and modeled  
412 groundwater level varies from  $0.15-4.02 \times 10^{-2}$  for GPS sites P544 and P303, respectively  
413 (Figure 5a-b; Table 1). In addition, we find a good correlation between the long-term  
414 subsidence and the modeled groundwater level at the selected GPS locations (Table 1).  $S_{kv}$   
415 computed from groundwater level and CS2 varies among the subbasins. The mean  $S_{kv}$  over  
416 the subbasins is  $5.89 \times 10^{-2}$ .



417

418 **Figure 5.** Computation of inelastic storage coefficient. (a) and (b) shows modeled groundwater  
419 level and vertical deformation from GPS at P304 and P545 (shown in Figure 1). (c) shows the

420 inelastic storage coefficients for subbasins computed from modeled groundwater level and  
 421 deformation data from CS-2 altimeter.

422

GPS	$S_{kv}$ (This study)	Correlation between groundwater level and deformation from GPS	$S_{kv}$ (Ojha et al., 2019)
P303	3.46	0.90	1.87
P304	0.9	0.96	1.38
P307	1.94	0.89	1.14
P544	0.15	0.85	0.19
P565	4.02	0.91	-
P566	0.86	0.86	0.76
P545	0.42	0.94	0.33
P563	0.38	0.96	-

423

424 Table 1. Computation of  $S_{kv}$  from modeled groundwater level and vertical deformation.  $S_{kv}$   
 425 from Ojha et al., (2019) is shown for reference

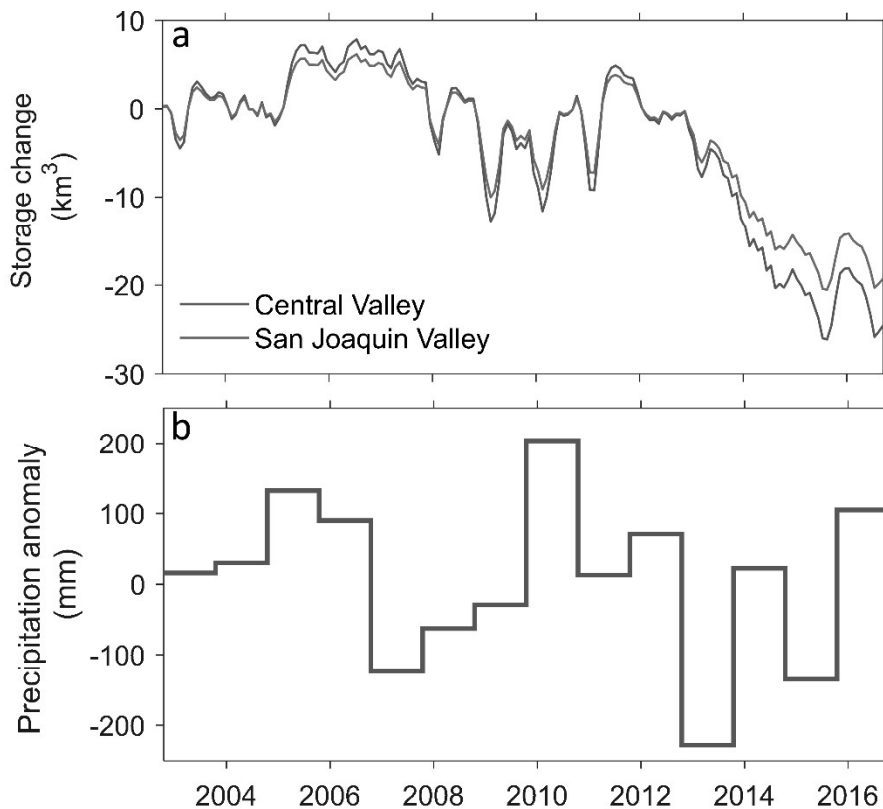
426

427

428 **4.3 Spatio-temporal variations of groundwater variations**

429 Central Valley lost approximately 30 km<sup>3</sup> of groundwater from October 2002 - September 2016  
 430 (Figure 6a). The most rapid decline in groundwater occurs during the two drought periods,  
 431 January 2007- December 2009, and October 2011 - September 2015 (Table). These periods of

432 decline usually follow or happen during phases of low/negative annual precipitation anomalies  
433 (Figure 6b). Periods of positive annual precipitation anomalies usually are followed by periods of  
434 increase in groundwater storage.



435  
436 **Figure 6.** (a) Temporal variations of groundwater storage in Central Valley and San Joaquin  
437 Valley (shown for comparison), and (b) annual precipitation anomalies in the Central Valley.

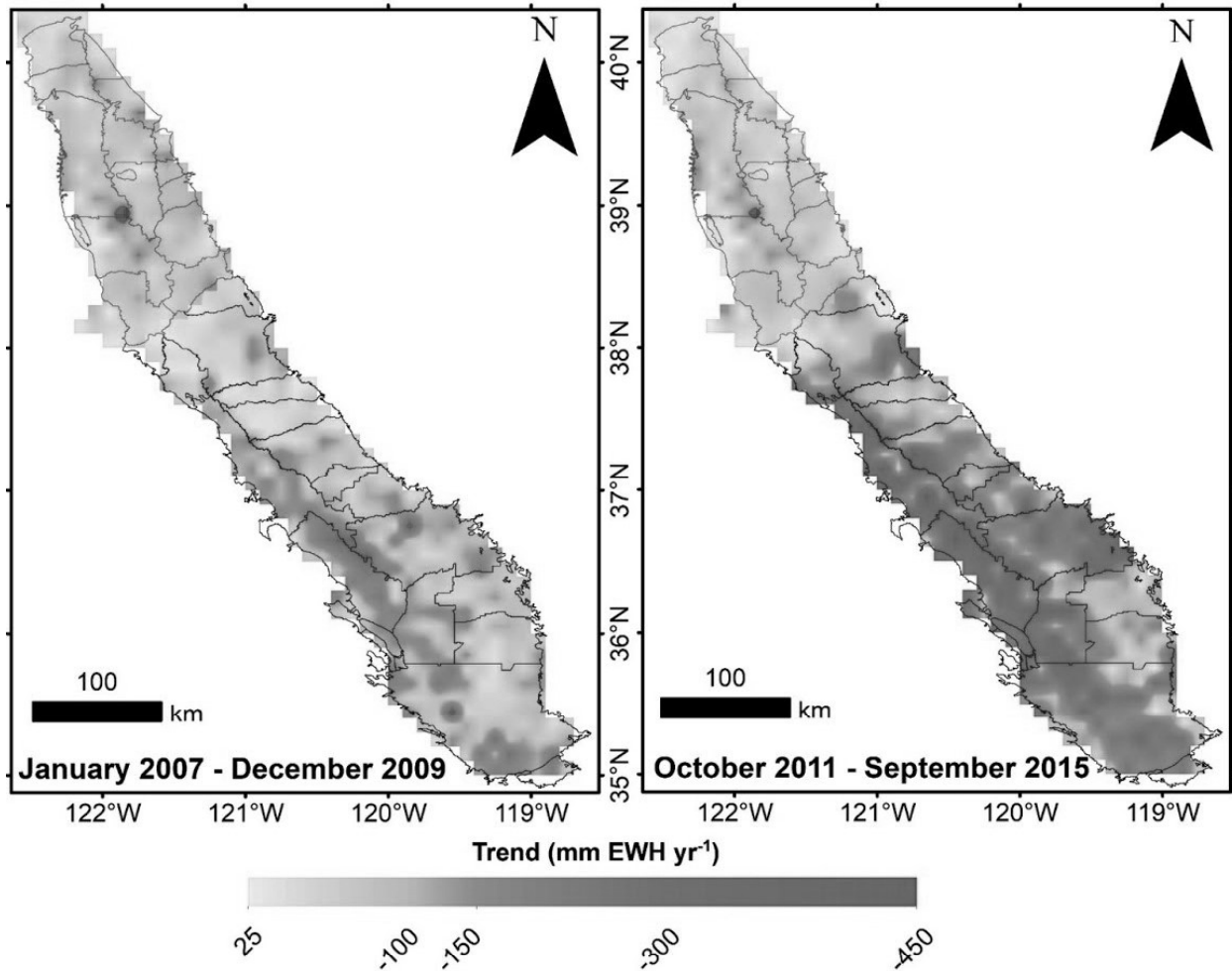
438  
439  
440  
441  
442

Time period	Annual groundwater volume loss (km <sup>3</sup> yr <sup>-1</sup> )		
	This Study	Previous Results	Study
April 2006 - September 2009	-5.1 ± 1.2	-7.8 ± 0.8	(Scanlon et al., 2012)
		-4.2 ± 0.3	(Xiao et al., 2017)
April 2006 – March 2010	-4.2 ± 1.0	-6.0 ± 1.5 -4.1 ± 0.2	(Famiglietti et al., 2011)
January 2007 – December 2009	-5.7 ± 1.2	-7.1 ± 2.4	(Ojha et al., 2018)
		-5.5 ± 0.3	(Xiao et al., 2017)
		-6	(Alam et al., 2021)
		-(3-10)	(Ahamed et al., 2022)
October 2011 – September 2015	-7.6 ± 1.5 (San Joaquin Valley only)	-6.1 * (San Joaquin Valley only)	(Ojha et al., 2019)
	-9.8 ± 1.7	-7	(Alam et al., 2021)
		-(6-17)	(Ahamed et al., 2022)
October 2012 – September 2016	-7.7 ± 1.8	-10.0 ± 0.2	(Xiao et al., 2017)

443 **Table 2.** Comparison of GWS loss obtained from this study with previously published estimates.

444

445 GWS declines over San Joaquin valley are more prominent than declines over Sacramento  
446 valley (Figure 7). The decline during the latter drought period can be seen in wider areas and  
447 have a higher magnitude compared to the declines during the former period. Groundwater  
448 depletion can be seen mainly in Tulare Lake, Tule, and Kern subbasins, although lower  
449 groundwater depletion can be observed in Kings, Westside, and Kaweah subbasins.



450

451 **Figure 7.** Spatial variations in modeled groundwater storage trends at 5-km resolution for (a)  
452 January 2007- December 2015 (b) October 2011–September 2015

453

454 **Discussion**

## 455        **1. Choice of predictor variables in ML modeling**

456        Several hydrological and geological datasets have been used in past studies for modeling  
457        groundwater storage variations in previous studies. These include temperature, precipitation,  
458        soil type, soil moisture, land cover, evapotranspiration, canopy water, and surface runoff  
459        (Jyolsna et al., 2021; Milewski et al., 2019; Seyoum et al., 2019; Sun et al., 2013; Yin et al.,  
460        2022). The choice of these predictors depends on the study area and type of aquifer and  
461        obviously on the availability of reliable data. For example, evapotranspiration is difficult to model  
462        reliably for heavily irrigated regions like Central Valley (Allen et al., 2011) and was not used.  
463        Surface water changes for Central Valley might be available at sufficient resolution through the  
464        Surface Water Ocean Topography (SWOT) mission to be launched after 2022. Several of the  
465        predictors chosen in this study, such as precipitation, temperature, topographic slope, and  
466        texture, have also been used in the numerical groundwater models as they hold importance for  
467        hydrological balances (Faunt, 2009; Faunt et al., 2016).

468        RF model also estimated that input data used in modeling has different importance for  
469        Sacramento and San Joaquin Valley (Figure 3b), suggesting that different processes are  
470        ongoing in the two regions. Texture or percentage of coarse-grained material is an important  
471        indicator of the lithological variations in Central Valley. While Sacramento valley shows fine-  
472        grained texture as it majorly consists of sediments derived from fine-grained volcanic rocks, San  
473        Joaquin Valley shows spatial variation in texture from east to west. The eastern region near the  
474        Sierra Nevada has coarser-grained sediments, making this region a good aquifer. The western  
475        part near the Coast Ranges has a fine-grained texture, being richer in shale. San Joaquin Valley  
476        and Tulare Basin consist of alternating layers of coarse and fine material, creating a mix of  
477        confined, unconfined, and semi-confined units.

478        Saturated hydraulic conductivity ( $K$ ) describes the ease with which water moves through the  
479        pore spaces in the soil and is considered an important quantity in groundwater modeling

480 (Sanchez-Villa et al., 2006). Its order of importance is second and third for Sacramento and San  
481 Joaquin valley based on permutation of OOB data. Together, hydraulic conductivity and texture  
482 provide important geological information about groundwater flow patterns in the whole Central  
483 Valley at high spatial resolutions and the removal of both predictors causes a significant  
484 increase in RMSE of models. Variations in topographic slopes lead to differences in  
485 groundwater recharge (Satapathy and Syed, 2015). Its importance is, however, lesser than  
486 other geological variables.

487 TWSA-SMA, though at coarse resolution, provides valuable information about the continuous  
488 spatio-temporal groundwater storage variations over the last decade and a half. However,  
489 removal of this predictor alone causes the most increase in RMSE for models built for  
490 Sacramento and San Joaquin valley. Based on OOB permutation, it is of mid-importance. The  
491 above two findings seem contradictory. However, they can be explained by the fact that this  
492 predictor has crucial information for modeling groundwater variations, though at the lowest  
493 resolution of all predictors. Therefore, the permutation of this predictor might not significantly  
494 affect the predictions, while its removal affects the modeling results.

495 Precipitation is the dominant source of groundwater recharge and is, therefore, most significant  
496 for determining groundwater level patterns in Sacramento Valley based on OOB permutation. In  
497 contrast, San Joaquin Valley majorly depends on other surface water sources for recharge and  
498 anthropogenic sources might influence the groundwater withdrawal significantly. Its significance  
499 is, therefore, least for San Joaquin Valley. However, based on the drop-column method,  
500 precipitation has the least impact if removed from modeling in both Sacramento and San  
501 Joaquin valley.

502 Temperature consists of seasonal signals, which might also help capture seasonal groundwater  
503 signals. It is the least important for San Joaquin valley based on OOB permutation. However, its  
504 removal significantly affects the accuracy of modeling in Sacramento valley.

505

506 **2. Accuracy of machine learning results**

507 Our study achieved high accuracy for both cross-validated and test data in Sacramento and San  
508 Joaquin valleys (Figure 3a). Therefore, we minimized the overfitting, which reduces the  
509 confidence of machine learning results (Roelofs, 2018). Overall results indicate excellent NSE  
510 coefficients at 0.94–0.97 for validation data, revealing superior model predictive capability.  
511 These results are similar to Agarwal (2020), that used only 180 wells for modeling in Central  
512 Valley using the Random Forest model. As our accuracy estimates are similar to Agarwal,  
513 (2020), we can conclude that Random Forest can accommodate additional data without  
514 sacrificing accuracy.

515 An earlier study in southern San Joaquin Valley by Miro and Famiglietti, (2018) also used ANN  
516 and therefore we compared similarities and differences between this study, Agarwal, (2020) and  
517 Miro and Famiglietti, (2018). Miro and Famiglietti (2018) obtained validation NSE ranging from  
518 0.039 to 0.751 when modeling annual groundwater storage variations in southern San Joaquin  
519 valley using ANN. We obtained a better validation NSE of 0.95 for San Joaquin Valley when  
520 modeling monthly groundwater variations using random forest. Even Agarwal (2020) obtained a  
521 validation NSE of 0.86 using ANN. This is despite the fact that our study used similar predictors  
522 such as precipitation, temperature, and topographic slope from the same source as Miro and  
523 Famiglietti, (2018). We have processed GRACE L2 data along with leakage correction, while  
524 Miro and Famiglietti, (2018) used GRACE L3 monthly mass grids. A possible reason for the  
525 lower accuracy in their study might be because they model groundwater storage for each year,  
526 leaving less spatio-temporal data for modeling groundwater storage. Miro and Famiglietti (2018)  
527 use kriging to interpolate groundwater level changes for each year, a process that might lead to  
528 further errors (Deutsch, 2003; Sun et al., 2009). Since these kriged groundwater levels were  
529 used for training the model, kriging errors can further propagate in the modeled groundwater



530 storage variations. The choice of geological variables like texture and/or hydraulic conductivity  
531 might have further improved the accuracy. Further, since Random Forest is less prone to  
532 overfitting compared to ANN (Agarwal, 2020), Miro and Famiglietti, (2018) could have  
533 considered random forest for comparison with their results.

534 We have directly used groundwater level as the output variable in ML modeling and then used  
535 the modeled results to compute groundwater storage. Several studies in the past have focused  
536 on groundwater level modeling and forecasting using fuzzy logic, ANN, Support Vector  
537 Machine, and other computational algorithms (see a comprehensive review by Rajaei et al.,  
538 (2019) and references therein). Nonetheless, several studies have been conducted lately on  
539 modeling groundwater storage using RF and other algorithms.

540 Jyolsna et al. (2021) obtained a correlation of 0.50-0.83 when modeling TWSA in different  
541 Indian aquifers using RF, while Seyoum and Milewski, (2017) found a correlation of 0.86 when  
542 modeling TWS in Northern High Plains using ANN. Koch et al., (2019) obtained a correlation of  
543 0.78 when modeling depth to shallow water table for aquifers in Denmark using RF. Seyoum et  
544 al., (2019) obtained an NSE value of 0.45 when downscaling groundwater level anomalies for  
545 glacial aquifers in Illinois using a two-stage boosted regression tree. Rahaman et al., (2020)  
546 downscaled GRACE-derived groundwater storage variations in Northern High Plains to 0.25°  
547 resolution and produced NSE in the range of 0.5-0.8 using RF. Although our study and past  
548 studies have used different output variables related to groundwater in machine learning  
549 modeling, better validation accuracy achieved in this study might also be attributed to  
550 improvements in model choice and model development as well as the choice of input predictors.  
551 The modeled groundwater level fits closely to the in-situ data from individual ground wells. They  
552 can capture the long-term decline in groundwater, accelerated depletion during the two drought  
553 periods, recovery during the wet years, and seasonal variations, which are essential for  
554 groundwater modeling in Central Valley (Ahamed et al., 2022).

555

### 556 **3. Spatio-temporal variations in groundwater storage**

557 The groundwater storage losses or drought 1 range from 27 km<sup>3</sup> (Scanlon et al., 2012) to 29  
558 km<sup>3</sup> (Ahamed et al., 2022), while losses for drought 2 are 71 km<sup>3</sup> (Ahamed et al., 2022).

559 Groundwater storage losses from the ensemble water balance method (Ahamed et al., 2022)  
560 range from 8 to 31 km<sup>3</sup> for drought 1 and vary from 22 to 67 km<sup>3</sup> for drought 2. Variations in the  
561 estimate are due to different combinations of remote sensing, in-situ, and model data used in  
562 the water balance approach. Xiao et al., (2017) estimated groundwater storage loss of 16.5 km<sup>3</sup>  
563 and 40.0 km<sup>3</sup> during drought 1 and 2, respectively, using the water balance approach, which  
564 also matched with the estimates from GRACE in their study. Ojha et al., (2018) estimated  
565 groundwater loss of  $21.32 \pm 7.2$  km<sup>3</sup> during drought 1. Ojha et al., (2019) estimated that San  
566 Joaquin valley lost  $24.2 \pm 9.3$  km<sup>3</sup> lost groundwater from October 2011 to September 2015  
567 based on GRACE data. Based on the GPS vertical deformation data, groundwater loss was  
568  $29.25 \pm 8.7$  km<sup>3</sup> for the same region and period (Ojha et al., 2019). Groundwater storage losses  
569 for droughts 1 and 2 are  $17.1 \pm 3.6$  and  $39.2 \pm 5.1$  km<sup>3</sup>, respectively, from this study which lie  
570 within the range of previous estimates.

571 There is significant variability of storage losses for similar time periods using similar  
572 approaches. The causes of the variations include different methods and datasets along with  
573 their errors. Scanlon et al., (2012) used a distributed specific yield ranging from 0.05-0.3 in their  
574 study to estimate groundwater storage variations from in-situ groundwater levels (Faunt, 2009).  
575 Since regions with high groundwater level declines in southern San Joaquin valley have higher  
576 specific yields, it might be one of the reasons for higher groundwater storage estimated by their  
577 study. Water balance approach also has errors related to input variables, such as  
578 evapotranspiration which was identified as the most uncertain variable (Xiao et al., 2017;  
579 Ahamed et al., 2022). Estimates of regional groundwater storage from in-situ groundwater level

580 data will require significant spatio-temporal interpolation due to issues with coverage in many  
581 regions (Figure 1). GRACE-derived TWS is also affected by several errors during data  
582 processing, which might also impact our machine learning model.

583

#### 584 **4. Comparison with vertical deformation data**

585 Several past studies have combined groundwater levels from in-situ wells with geodetic  
586 observations from GPS and InSAR to obtain inelastic storage coefficient. Calculated inelastic  
587 storage coefficients for individual subbasins in southern San Joaquin valley from this study is  
588 comparable to past studies (Ojha et al., 2018). Ojha et al., (2018) computed  $S_{kv}$  of  $4.08 \times 10^{-2}$   
589 for the whole of Central Valley, with San Joaquin having a higher  $S_{kv}$ . Ojha et al., (2019)  
590 computed a mean value of as  $2.3 \times 10^{-2}$ , while Smith et al., (2017) reported a computed mean  
591 with the range of  $2.3 \times 10^{-2}$  -  $11.0 \times 10^{-2}$  using estimates of aquifer compaction modeling for the  
592 San Joaquin Valley. These estimates compare to  $5.8 \times 10^{-2}$  from our study.

593 At GPS sites, P304 and P545, vertical deformation can be seen mostly in times of drought with  
594 the groundwater level dropping. Between drought periods, the groundwater level was rising due  
595 to the availability of surface water; hence, little deformation occurred. Further, at the well site  
596 near P304, the lowest water level was recorded in 1992 at 45 m below the land surface (Faunt  
597 et al., 2016). At the end of drought1, and most of the drought 2, modeled groundwater level at  
598 the site of P304 was below the previous lowest level (pre-consolidation stress level). The  
599 correlation between subsidence and long-term groundwater levels suggests that groundwater  
600 overdraft was the cause of the subsidence (Liu et al., 2019). Further analysis could be done with  
601 long-term modeled groundwater level data and vertical deformation data for other sites to  
602 understand the aquifer compaction. Higher groundwater depletion can be combined with  
603 geological models to study sites that might be further vulnerable to subsidence.

604 Significant groundwater depletion can be seen for subbasins in the Tulare basin and western  
605 San Joaquin valley for both the droughts. These regions have also been subjected to  
606 subsidence (Faunt et al., 2016, Sneed et al., 2013; Farr et al., 2015). It is an expected  
607 consequence because this region requires water for *intensive* irrigation and drinking water  
608 needs. Due to climate extremes such as droughts, surface water has dwindled over the years.  
609 Consequently, groundwater from the deeper confined aquifers is usually extracted and the  
610 overlying aquitard belonging to the Corcoran clay layer undergoes compaction. Due to the  
611 continued groundwater losses in this region exacerbated during droughts, irreversible  
612 compaction of the clay layers results in subsidence signals and might reflect the permanent loss  
613 in groundwater (Smith et al., 2017; Vasco et al., 2019).

614 It is important to note that the groundwater storage variations reflect the balance between  
615 groundwater recharge and abstractions in an area or region and directly reflect groundwater  
616 depletion. Magnitude and rate of subsidence, on the other hand, might also depend on the  
617 hydraulic and mechanical properties of the aquifer along with the past stress regime in the region.  
618 Our results are, therefore, an important contribution to the study of localized groundwater  
619 variations in the Central Valley for the study period longer than one and a half decades.

620

621

## 622 **5. Future perspectives**

623 The approach presented here has some limitations. The Random forests, like most of the  
624 other machine learning models, cannot predict reliably outside the training range (Hengl et al.,  
625 2019). We might not be able to use the model developed here in a new region with different  
626 geology and groundwater conditions. We will have to build a new model which can be applied to  
627 a specific region. However, this limitation is also applicable to numerical groundwater models or

628 the water balance approach. We propose building deep learning networks incorporating larger  
629 datasets and wider regions to model more complex variations in the future.

630 Further, unlike the water balance method of Ahamed et al., (2022), which predicted groundwater  
631 storage variations for 2002-2020 in Central Valley, our method is currently limited by the  
632 temporal coverage of the GRACE. The GRACE mission operated from 2002-2017, followed by  
633 a gap of 1 year, after which GRACE-FO was launched. Several studies have filled the data gap  
634 using deep learning (e.g., Uz et al., 2021), and modeled GRACE data from such studies can be  
635 used to extend the study for a longer time.

## 636 **Conclusions**

637 This study advances the application of remote sensing data in the field of hydrological  
638 sciences by demonstrating an effective and improved downscaling of GRACE-estimated  
639 groundwater storage variations in Central Valley to a spatial resolution of 5 km using Random  
640 Forest ML approach and other hydrologic, meteorologic, and geologic datasets. We applied it in  
641 the Central Valley region, which has developed an ever-increasing groundwater demand for  
642 irrigation given the lack of surface water supplies within most parts and has also been impacted  
643 by two droughts during our study period. Making the information about local-scale groundwater  
644 variations across Central Valley will be crucial to help twitch the groundwater management as  
645 per the plans of SGMA.

646 We obtained good modeling accuracy for San Joaquin and Sacramento Valley, proving that  
647 Random Forest is a robust machine learning model for such applications. We obtained similar  
648 or better prediction accuracy than other studies implementing machine learning to quantify  
649 groundwater storage variations, possibly because of the choice of predictors, choice and  
650 development of machine learning models. Development of better models, including deep

651 learning, can further improve modeling. However, the Random Forest model developed here is  
652 suited for studies wherein predictor importance is required.

653 We also suggest new approaches for validating machine learning modeled results by  
654 comparing long-term modeled groundwater level changes with vertical deformation from GPS  
655 and CS-2 altimeter. The produced inelastic storage coefficient is an important aquifer  
656 mechanical reflecting deformation caused due to groundwater withdrawal. Since 2014, Sentinel-  
657 1 can provide information about continuous vertical deformation using Interferometric Synthetic  
658 Aperture Radar (InSAR) technique. Using a similar approach as in this study, new information  
659 about the aquifer dynamics using Sentinel-1, GRACE-FO, and in-situ groundwater level data  
660 can be generated.

661 Central Valley exhibits groundwater loss of  $\sim 30 \text{ km}^3$  during October 2002 - September 2016;  
662 however, there are periods of depletion and recharge during or followed by precipitation.  
663 Maximum amount of groundwater depletion occurs during the drought of January 2007-  
664 December 2009 and October 2011-September 2015, with rates of  $-5.7 \pm 1.2$  and  $-9.8 \pm 1.7 \text{ km}^3$   
665  $\text{yr}^{-1}$ , respectively. We produced groundwater depletion maps at 5 km resolution for these  
666 drought periods that can identify groundwater overdraft areas. These areas have also exhibited  
667 land subsidence.

668 We conclude that the resulting modeled time series of groundwater storage variations at 5 km  
669 resolution over a decade and a half time period is effective for practical groundwater resources  
670 management.

671

672

673

674

675

676

677 **References**

678 Adamowski, J., Chan, H.F., 2011. A wavelet neural network conjunction model for groundwater  
679 level forecasting. *Journal of Hydrology* 407, 28–40.

680 <https://doi.org/10.1016/J.JHYDROL.2011.06.013>

681 Agarwal, V. (2021). Machine Learning Applications for Downscaling Groundwater Storage  
682 Changes Integrating Satellite Gravimetry and Other Observations [Doctoral dissertation,  
683 Ohio State University]. OhioLINK Electronic Theses and Dissertations Center.

684 [http://rave.ohiolink.edu/etdc/view?acc\\_num=osu1609914912574523](http://rave.ohiolink.edu/etdc/view?acc_num=osu1609914912574523)

685 A, G., Wahr, J., Zhong, S., 2013. Computations of the viscoelastic response of a 3-D  
686 compressible Earth to surface loading: an application to Glacial Isostatic Adjustment in  
687 Antarctica and Canada. *Geophysical Journal International* 192, 557–572.

688 <https://doi.org/10.1093/gji/ggs030>

689 Ahamed, A., Knight, R., Alam, S., Pauloo, R., Melton, F., 2022. Assessing the utility of remote  
690 sensing data to accurately estimate changes in groundwater storage. *Science of The Total  
691 Environment* 807, 150635. <https://doi.org/10.1016/J.SCITOTENV.2021.150635>

692 Alam, S., Gebremichael, M., Ban, Z., Scanlon, B.R., Senay, G., Lettenmaier, D.P., 2021b. Post-  
693 Drought Groundwater Storage Recovery in California's Central Valley. *Water Resources  
694 Research* 57, e2021WR030352. <https://doi.org/10.1029/2021WR030352>

695 Alam, S., Gebremichael, M., Li, R., Dozier, J., Lettenmaier, D.P., 2020. Can Managed Aquifer  
696 Recharge Mitigate the Groundwater Overdraft in California's Central Valley? Water  
697 Resources Research 56, e2020WR027244. <https://doi.org/10.1029/2020WR027244>

698 Alley, W.M., Konikow, L.F., 2015. Bringing GRACE Down to Earth. Groundwater 53, 826–829.  
699 <https://doi.org/10.1111/gwat.12379>

700 Bertoldi, G.L., 1989. Ground-water resources of the Central Valley of California.

701 Biau, G., Scornet, E., 2016. A random forest guided tour. Test 25, 197–227.  
702 <https://doi.org/10.1007/S11749-016-0481-7/FIGURES/4>

703 Bierkens, M.F.P., Wada, Y., 2019. Non-renewable groundwater use and groundwater depletion:  
704 a review. Environmental Research Letters 14, 063002. [https://doi.org/10.1088/1748-](https://doi.org/10.1088/1748-9326/AB1A5F)  
705 [9326/AB1A5F](https://doi.org/10.1088/1748-9326/AB1A5F)

706 Breiman, L., 2001. Random forests. Machine Learning 45, 5–32.  
707 <https://doi.org/10.1023/A:1010933404324>

708 Butler, J.J., Stotler, R.L., Whittemore, D.O., Reboulet, E.C., 2013. Interpretation of Water Level  
709 Changes in the High Plains Aquifer in Western Kansas. Groundwater 51, 180–190.  
710 <https://doi.org/10.1111/J.1745-6584.2012.00988.X>

711 Castellazzi, P., Martel, R., Galloway, D.L., Longuevergne, L., Rivera, A., 2016. Assessing  
712 groundwater depletion and dynamics using GRACE and InSAR: Potential and limitations.  
713 Groundwater 54, 768–780. <https://doi.org/10.1111/gwat.12453>

714 Chen, J., Li, J., Zhang, Z., Ni, S., 2014. Long-term groundwater variations in Northwest India  
715 from satellite gravity measurements. Global and Planetary Change 116, 130–138.  
716 <https://doi.org/10.1016/j.gloplacha.2014.02.007>



717 Chen, C., He, W., Zhou, H., Xue, Y., Zhu, M., 2020. A comparative study among machine  
718 learning and numerical models for simulating groundwater dynamics in the Heihe River  
719 Basin, northwestern China. *Scientific Reports* 10. [https://doi.org/10.1038/s41598-020-](https://doi.org/10.1038/s41598-020-60698-9)  
720 [60698-9](https://doi.org/10.1038/s41598-020-60698-9)

721 Chen, L., He, Q., Liu, K., Li, J., Jing, C., 2019. Downscaling of GRACE-Derived Groundwater  
722 Storage Based on the Random Forest Model. *Remote Sensing* 11, 2979.  
723 <https://doi.org/10.3390/RS11242979>

724 Cheng, M.K., Ries, J.R., 2018. Monthly estimates of C20 from 5 SLR satellites based on  
725 GRACE RL06 models.

726 Daly, C., Halbleib, M., Smith, J.I., Gibson, W.P., Doggett, M.K., Taylor, G.H., Curtis, J., Pasteris,  
727 P.P., 2008. Physiographically sensitive mapping of climatological temperature and  
728 precipitation across the conterminous United States. *International Journal of Climatology*  
729 28, 2031–2064. <https://doi.org/10.1002/joc.1688>

730 Department of Water Resources California Statewide Groundwater Elevation Monitoring (DWR  
731 CASGEM), 2021b. Periodic groundwater level measurements. [Data file].  
732 <https://data.cnra.ca.gov/dataset/periodic-groundwater-level-measurements>.

733 Department of Water Resources California Statewide Groundwater Elevation Monitoring (DWR  
734 CASGEM), 2021b. Continuous groundwater level measurements. [Data file].  
735 <https://data.cnra.ca.gov/dataset/continuous-groundwater-level-measurements>.

736 Dramsch, J.S., 2020. 70 years of machine learning in geoscience in review. *Advances in*  
737 *Geophysics* 61, 1–55. <https://doi.org/10.1016/BS.AGPH.2020.08.002>

738 Erban, L.E., Gorelick, S.M., Zebker, H.A., 2014. LETTER • OPEN ACCESS Groundwater  
739 extraction, land subsidence, and sea-level rise in the Mekong Delta, Vietnam.  
740 <https://doi.org/10.1088/1748-9326/9/8/084010>

741 Famiglietti, J.S., 2014. The global groundwater crisis. *Nature Climate Change* 2014 4:11 4,  
742 945–948. <https://doi.org/10.1038/nclimate2425>

743 Famiglietti, J.S., Lo, M., Ho, S.L., Bethune, J., Anderson, K.J., Syed, T.H., Swenson, S.C., de  
744 Linage, C.R., Rodell, M., 2011. Satellites measure recent rates of groundwater depletion in  
745 California's Central Valley. *Geophysical Research Letters* 38, 2010GL046442.  
746 <https://doi.org/10.1029/2010GL046442>

747 Farr, T.G., Jones, C., Liu, Z., 2015. Progress Report: Subsidence in the Central Valley,  
748 California.

749 Farr, T.G., Liu, Z., 2014. Monitoring Subsidence Associated with Groundwater Dynamics in the  
750 Central Valley of California Using Interferometric Radar, in: *Remote Sensing of the*  
751 *Terrestrial Water Cycle*. Wiley Blackwell, pp. 397–406.  
752 <https://doi.org/10.1002/9781118872086.ch24>

753 Faunt, C.C., 2009. Groundwater Availability of the Central Valley Aquifer, California: U.S.  
754 Geological Survey Professional Paper, 1766.

755 Faunt, C.C., Belitz, K., Hanson, R.T., 2009. Development of a three-dimensional model of  
756 sedimentary texture in valley-fill deposits of Central Valley, California, USA. *Hydrogeology*  
757 *Journal* 2009 18:3 18, 625–649. <https://doi.org/10.1007/S10040-009-0539-7>

758 Faunt, C.C., Sneed, M., 2015. Water availability and subsidence in California's Central Valley.  
759 San Francisco Estuary and Watershed Science 13.  
760 <https://doi.org/10.15447/SFEWS.2015V13ISS3ART4>

761 Faunt, C.C., Sneed, M., Traum, J., Brandt, J.T., 2016. Water availability and land subsidence in  
762 the Central Valley, California, USA. Hydrogeology Journal 24, 675–684.  
763 <https://doi.org/10.1007/s10040-015-1339-x>

764 Feng, W., 2019. GRAMAT: a comprehensive Matlab toolbox for estimating global mass  
765 variations from GRACE satellite data. Earth Science Informatics 12, 389–404.  
766 <https://doi.org/10.1007/s12145-018-0368-0>

767 Feurer, M., Hutter, F., 2019. Hyperparameter Optimization, in: Automated Machine Learning.  
768 Springer, Cham, pp. 3–33. [https://doi.org/10.1007/978-3-030-05318-5\\_1](https://doi.org/10.1007/978-3-030-05318-5_1)

769 Fowler, H.J., Wilby, R.L., 2007. Beyond the downscaling comparison study. International  
770 Journal of Climatology 27, 1543–1545. <https://doi.org/10.1002/joc.1616>

771 Frappart, F., Ramillien, G., 2018. Monitoring Groundwater Storage Changes Using the Gravity  
772 Recovery and Climate Experiment (GRACE) Satellite Mission: A Review. Remote Sensing  
773 10, 829. <https://doi.org/10.3390/rs10060829>

774 Hawkins, D.M., Basak, S.C., Mills, D., 2003. Assessing model fit by cross-validation. Journal of  
775 Chemical Information and Computer Sciences 43, 579–586.  
776 <https://doi.org/10.1021/CI025626I/ASSET/IMAGES/LARGE/CI025626IF00006.JPEG>

777 Hengl, T., Nussbaum, M., Wright, M.N., Heuvelink, G.B.M., Gräler, B., 2018. Random forest as  
778 a generic framework for predictive modeling of spatial and spatio-temporal variables. PeerJ  
779 2018. <https://doi.org/10.7717/PEERJ.5518>

780 Hoffmann, J., Galloway, D.L., Zebker, H.A., 2003. Inverse modeling of interbed storage  
781 parameters using land subsidence observations, Antelope Valley, California. *Water*  
782 *Resources Research* 39. <https://doi.org/10.1029/2001WR001252>

783 Jasechko, S., Perrone, D., 2020. California's Central Valley Groundwater Wells Run Dry During  
784 Recent Drought. *Earth's Future* 8, e2019EF001339. <https://doi.org/10.1029/2019EF001339>

785 Jekeli, C., 1981. Modifying Stokes' function to reduce the error of geoid undulation  
786 computations. *Journal of Geophysical Research* 86, 6985.  
787 <https://doi.org/10.1029/JB086iB08p06985>

788 Jyolsna, P.J., Kambhammettu, B.V.N.P., Gorugantula, S., 2021. Application of random forest  
789 and multi-linear regression methods in downscaling GRACE derived groundwater storage  
790 changes. *Hydrological Sciences Journal* 66, 874–887.  
791 <https://doi.org/10.1080/02626667.2021.1896719>

792 Koch, J., Berger, H., Henriksen, H.J., Sonnenborg, T.O., 2019. Modelling of the shallow water  
793 table at high spatial resolution using random forests. *Hydrology and Earth System*  
794 *Sciences* 23, 4603–4619. <https://doi.org/10.5194/HESS-23-4603-2019>

795 Konikow, L.F., 2015. Long-Term Groundwater Depletion in the United States. *Groundwater* 53,  
796 2–9. <https://doi.org/10.1111/gwat.12306>

797 Konikow, L.F., Kendy, E., 2005. Groundwater depletion: A global problem. *Hydrogeology*  
798 *Journal* 13, 317–320. <https://doi.org/10.1007/s10040-004-0411-8>

799 Kuhn, M., Johnson, K., 2013. Over-Fitting and Model Tuning, in: *Applied Predictive Modeling*.  
800 Springer New York, pp. 61–92. [https://doi.org/10.1007/978-1-4614-6849-3\\_4](https://doi.org/10.1007/978-1-4614-6849-3_4)

801 Landerer, F.W., Swenson, S.C., 2012. Accuracy of scaled GRACE terrestrial water storage  
802 estimates. *Water Resources Research* 48, 4531. <https://doi.org/10.1029/2011WR011453>

803 Liu, Z., Liu, P.-W., Massoud, E., Farr, T.G., Lundgren, P., Famiglietti, J.S., 2019. Monitoring  
804 Groundwater Change in California's Central Valley Using Sentinel-1 and GRACE  
805 Observations. *Geosciences (Basel)* 9, 436. <https://doi.org/10.3390/geosciences9100436>

806 Liu, Z., Liu, P.-W., Massoud, E., Farr, T.G., Lundgren, P., Famiglietti, J.S., 2019. Monitoring  
807 Groundwater Change in California's Central Valley Using Sentinel-1 and GRACE  
808 Observations. *Geosciences (Basel)* 9, 436. <https://doi.org/10.3390/geosciences9100436>

809 Lo, M., Famiglietti, J.S., 2013. Irrigation in California's Central Valley strengthens the  
810 southwestern U.S. water cycle. *Geophysical Research Letters* 40, 301–306.  
811 <https://doi.org/10.1002/grl.50108>

812 Mehrnegar, N., Jones, O., Singer, M.B., Schumacher, M., Jagdhuber, T., Scanlon, B.R., Rateb,  
813 A., Forootan, E., 2021. Exploring groundwater and soil water storage changes across the  
814 CONUS at 12.5 km resolution by a Bayesian integration of GRACE data into W3RA.  
815 *Science of The Total Environment* 758, 143579.  
816 <https://doi.org/10.1016/J.SCITOTENV.2020.143579>

817 Miro, M., Famiglietti, J., 2018. Downscaling GRACE Remote Sensing Datasets to High-  
818 Resolution Groundwater Storage Change Maps of California's Central Valley. *Remote  
819 Sensing* 10, 143. <https://doi.org/10.3390/rs10010143>

820 Molinaro, A.M., Simon, R., Pfeiffer, R.M., 2005. Prediction error estimation: a comparison of  
821 resampling methods. *Bioinformatics* 21, 3301–3307.  
822 <https://doi.org/10.1093/BIOINFORMATICS/BTI499>

823 Nash, J.E., Sutcliffe, J. V., 1970. River flow forecasting through conceptual models part I — A  
824 discussion of principles. *Journal of Hydrology* 10, 282–290. [https://doi.org/10.1016/0022-](https://doi.org/10.1016/0022-1694(70)90255-6)  
825 [1694\(70\)90255-6](https://doi.org/10.1016/0022-1694(70)90255-6)

826 Nourani, V., Hosseini Baghanam, A., Adamowski, J., Kisi, O., 2014. Applications of hybrid  
827 wavelet–Artificial Intelligence models in hydrology: A review. *Journal of Hydrology* 514,  
828 358–377. <https://doi.org/10.1016/J.JHYDROL.2014.03.057>

829 Ojha, C., Shirzaei, M., Werth, S., Argus, D.F., Farr, T.G., 2018. Sustained Groundwater Loss in  
830 California’s Central Valley Exacerbated by Intense Drought Periods. *Water Resources*  
831 *Research* 54, 4449–4460. <https://doi.org/10.1029/2017WR022250>

832 Ojha, C., Werth, S., Shirzaei, M., 2019. Groundwater Loss and Aquifer System Compaction in  
833 San Joaquin Valley During 2012–2015 Drought. *Journal of Geophysical Research: Solid*  
834 *Earth* 124, 3127–3143. <https://doi.org/10.1029/2018JB016083>

835 Parr, T., Wilson, J.D., Hamrick, J., 2020. Nonparametric Feature Impact and Importance. *arXiv*  
836 1–17.

837 Parr, T., Wilson, J.D., Hamrick, J., n.d. Nonparametric Feature Impact and Importance.

838 Probst, P., Boulesteix, A.L., 2017. To tune or not to tune the number of trees in random forest?  
839 *Journal of Machine Learning Research* 18, 1–8. <https://doi.org/10.48550/arxiv.1705.05654>

840 Rahaman, M., Thakur, B., Kalra, A., Li, R., Maheshwari, P., 2019. Estimating High-Resolution  
841 Groundwater Storage from GRACE: A Random Forest Approach. *Environments* 6, 63.  
842 <https://doi.org/10.3390/environments6060063>

843 Rajaei, T., Ebrahimi, H., Nourani, V., 2019. A review of the artificial intelligence methods in  
844 groundwater level modeling. *Journal of Hydrology* 572, 336–351.  
845 <https://doi.org/10.1016/J.JHYDROL.2018.12.037>

846 Rodell, M., Velicogna, I., Famiglietti, J.S., 2009. Satellite-based estimates of groundwater  
847 depletion in India. *Nature* 460, 999–1002. <https://doi.org/10.1038/NATURE08238>

848 Roelofs, R., 2019. *Measuring Generalization and Overfitting in Machine Learning*. University of  
849 California, Berkeley.

850 Sanchez-Vila, X., Guadagnini, A., Carrera, J., 2006. Representative hydraulic conductivities in  
851 saturated groundwater flow. *Reviews of Geophysics* 44, 3002.  
852 <https://doi.org/10.1029/2005RG000169>

853 Satapathy, I., Syed, T.H., 2015. Characterization of groundwater potential and artificial recharge  
854 sites in Bokaro District, Jharkhand (India), using remote sensing and GIS-based  
855 techniques. *Environmental Earth Sciences* 74, 4215–4232. [https://doi.org/10.1007/S12665-](https://doi.org/10.1007/S12665-015-4474-8/TABLES/10)  
856 [015-4474-8/TABLES/10](https://doi.org/10.1007/S12665-015-4474-8/TABLES/10)

857 Scanlon, B.R., Longuevergne, L., Long, D., 2012. Ground referencing GRACE satellite  
858 estimates of groundwater storage changes in the California Central Valley, USA. *Water*  
859 *Resources Research* 48. <https://doi.org/10.1029/2011WR011312>

860 Schumacher, M., Forootan, E., van Dijk, A.I.J.M., Müller Schmied, H., Crosbie, R.S., Kusche, J.,  
861 Döll, P., 2018. Improving drought simulations within the Murray-Darling Basin by combined  
862 calibration/assimilation of GRACE data into the WaterGAP Global Hydrology Model.  
863 *Remote Sensing of Environment* 204, 212–228. <https://doi.org/10.1016/J.RSE.2017.10.029>

864 Seyoum, W.M., Milewski, A.M., 2017. Improved methods for estimating local terrestrial water  
865 dynamics from GRACE in the Northern High Plains. *Advances in Water Resources* 110,  
866 279–290. <https://doi.org/10.1016/j.advwatres.2017.10.021>

867 Siebert, S., Henrich, V., Frenken, K., Burke, J., 2010. Update of the Global Map of Irrigation  
868 Areas to version 5.

869 Siebert, S., Henrich, V., Frenken, K., Burke, J., n.d. Update of the Global Map of Irrigation Areas  
870 to version 5.

871 Smith, R., Knight, R., Fendorf, S., 2018. Overpumping leads to California groundwater arsenic  
872 threat. *Nature Communications* 9, 1–6. <https://doi.org/10.1038/s41467-018-04475-3>

873 Smith, R.G., Knight, R., Chen, J., Reeves, J.A., Zebker, H.A., Farr, T., Liu, Z., 2017. Estimating  
874 the permanent loss of groundwater storage in the southern San Joaquin Valley, California.  
875 *Water Resources Research* 53, 2133–2148. <https://doi.org/10.1002/2016WR019861>

876 Snoek, J., Larochelle, H., Adams, R.P., 2012. Practical Bayesian optimization of machine  
877 learning algorithms, in: *Advances in Neural Information Processing Systems*. pp. 2951–  
878 2959.

879 Sun, A.Y., 2013. Predicting groundwater level changes using GRACE data. *Water Resources*  
880 *Research* 49, 5900–5912. <https://doi.org/10.1002/WRCR.20421>

881 Swenson, S., Chambers, D., Wahr, J., 2008. Estimating geocenter variations from a  
882 combination of GRACE and ocean model output. *Journal of Geophysical Research: Solid*  
883 *Earth* 113, 8410. <https://doi.org/10.1029/2007JB005338>

884 Swenson, S., Wahr, J., 2006. Post-processing removal of correlated errors in GRACE data.  
885 *Geophysical Research Letters* 33, L08402. <https://doi.org/10.1029/2005GL025285>



886 Taylor, C.J., Alley, W.M., 2001. Ground-water-level monitoring and the importance of long-term  
887 water-level data, Circular. <https://doi.org/10.3133/CIR1217>

888 Taylor, R.G., Scanlon, B., Döll, P., Rodell, M., van Beek, R., Wada, Y., Longuevergne, L.,  
889 Leblanc, M., Famiglietti, J.S., Edmunds, M., Konikow, L., Green, T.R., Chen, J., Taniguchi,  
890 M., Bierkens, M.F.P., Macdonald, A., Fan, Y., Maxwell, R.M., Yechieli, Y., Gurdak, J.J.,  
891 Allen, D.M., Shamsudduha, M., Hiscock, K., Yeh, P.J.F., Holman, I., Treidel, H., 2012.  
892 Ground water and climate change. *Nature Climate Change* 2012 3:4 3, 322–329.  
893 <https://doi.org/10.1038/nclimate1744>

894 Thomas, B.F., Famiglietti, J.S., Landerer, F.W., Wiese, D.N., Molotch, N.P., Argus, D.F., 2017.  
895 GRACE Groundwater Drought Index: Evaluation of California Central Valley groundwater  
896 drought. *Remote Sensing of Environment* 198, 384–392.  
897 <https://doi.org/10.1016/J.RSE.2017.06.026>

898 Tyralis, H., Papacharalampous, G., 2017. Variable Selection in Time Series Forecasting Using  
899 Random Forests. *Algorithms* 2017, Vol. 10, Page 114 10, 114.  
900 <https://doi.org/10.3390/A10040114>

901 Tyralis, H., Papacharalampous, G., Langousis, A., 2019. A Brief Review of Random Forests for  
902 Water Scientists and Practitioners and Their Recent History in Water Resources. *Water*  
903 2019, Vol. 11, Page 910 11, 910. <https://doi.org/10.3390/W11050910>

904 USGS Professional Paper 1766: Groundwater Availability of the Central Valley Aquifer,  
905 California [WWW Document], n.d. URL <https://pubs.usgs.gov/pp/1766/> (accessed 4.1.21).

906 Vasco, D.W., Farr, T.G., Jeanne, P., Doughty, C., Nico, P., 2019. Satellite-based monitoring of  
907 groundwater depletion in California's Central Valley. *Scientific Reports* 9, 1–14.  
908 <https://doi.org/10.1038/s41598-019-52371-7>

909 Wada, Y., van Beek, L.P.H., van Kempen, C.M., Reckman, J.W.T.M., Vasak, S., Bierkens,  
910 M.F.P., 2010. Global depletion of groundwater resources. *Geophysical Research Letters*  
911 37. <https://doi.org/10.1029/2010GL044571>

912 Wada, Y., Wisser, D., Bierkens, M.F.P., 2014. Global modeling of withdrawal, allocation and  
913 consumptive use of surface water and groundwater resources. *Earth System Dynamics* 5,  
914 15–40. <https://doi.org/10.5194/ESD-5-15-2014>

915 Wahr, J., Molenaar, M., Bryan, F., 1998. Time variability of the Earth's gravity field: Hydrological  
916 and oceanic effects and their possible detection using GRACE. *Journal of Geophysical*  
917 *Research: Solid Earth* 103, 30205–30229. <https://doi.org/10.1029/98JB02844>

918 Wahr, J., Swenson, S., Velicogna, I., 2006. Accuracy of GRACE mass estimates. *Geophysical*  
919 *Research Letters* 33, L06401. <https://doi.org/10.1029/2005GL025305>

920 Williamson, A.K., Prudic, D.E., Swain, L.A., 1989. Ground-water flow in the Central Valley,  
921 California: Professional Paper 1401-D.

922 Xiao, M., Koppa, A., Mekonnen, Z., Pagán, B.R., Zhan, S., Cao, Q., Aierken, A., Lee, H.,  
923 Lettenmaier, D.P., 2017. How much groundwater did California's Central Valley lose during  
924 the 2012-2016 drought? *Geophysical Research Letters* 44, 4872–4879.  
925 <https://doi.org/10.1002/2017GL073333>

926 Yang, T.-Y., 2020. Satellite Altimetry Applications on Lake Ice Thickness and Land Subsidence.  
927 The Ohio State University.

928 Yin, W., Fan, Z., Tangdamrongsub, N., Hu, L., Zhang, M., 2021a. Comparison of physical and  
929 data-driven models to forecast groundwater level changes with the inclusion of GRACE: a

930 case study over the state of Victoria, Australia. J Hydrol 602, 126735.  
931 <https://doi.org/10.1016/j.jhydrol.2021.126735>

932 Yin, W., Fan, Z., Tangdamrongsub, N., Hu, L., Zhang, M., 2021b. Comparison of physical and  
933 data-driven models to forecast groundwater level changes with the inclusion of GRACE – A  
934 case study over the state of Victoria, Australia. Journal of Hydrology 602, 126735.  
935 <https://doi.org/10.1016/J.JHYDROL.2021.126735>

936 Yin, W., Zhang, G., Liu, F., Zhang, D., Zhang, X., Chen, S., 2022. Improving the spatial  
937 resolution of GRACE-based groundwater storage estimates using a machine learning  
938 algorithm and hydrological model. Hydrogeology Journal 30, 947–963.  
939 <https://doi.org/10.1007/S10040-021-02447-4/FIGURES/11>

940 Zektser, Igor S., Everett, L.G., 2004. Groundwater resources of the world and their use,  
941 UNESCO IHP-VI series on groundwater no. 6. Paris, France: UNESCO.

942 Zhang, Y., Schaap, M.G., Zha, Y., 2018. A High-Resolution Global Map of Soil Hydraulic  
943 Properties Produced by a Hierarchical Parameterization of a Physically Based Water  
944 Retention Model. Water Resources Research 54, 9774–9790.  
945 <https://doi.org/10.1029/2018WR023539>

946

947